Cement and Concrete Research 40 (2010) 137–145

Contents lists available at ScienceDirect

Cement and Concrete Research

journal homepage: http://ees.elsevier.com/CEMCON/default.asp

Electrical Resistance Tomography imaging of concrete

Kimmo Karhunen [a], Aku Seppänen [a,*], Anssi Lehikoinen [a], Paulo J.M. Monteiro [b], Jari P. Kaipio [a,c]

[a] Department of Physics, University of Kuopio, P.O. Box 1627, FIN-70211 Kuopio, Finland
[b] Department of Civil and Environmental Engineering, University of California Berkeley, California, United States
[c] Department of Mathematics, University of Auckland, Auckland, New Zealand

ARTICLE INFO

Article history:
Received 31 March 2009
Accepted 27 August 2009

Keywords:
Concrete (E)
Electrical properties (C)
Crack detection (B)
Non-destructive testing

ABSTRACT

We apply Electrical Resistance Tomography (ERT) for three dimensional imaging of concrete. In ERT, alternating currents are injected into the target using an array of electrodes attached to the target surface, and the resulting voltages are measured using the same electrodes. These boundary measurements are used for reconstructing the internal (3D) conductivity distribution of the target. In reinforced concrete, the metallic phases (reinforcing bars and fibers), cracks and air voids, moisture gradients, and the chloride distribution in the matrix carry contrast with respect to conductivity. While electrical measurements have been widely used to characterize the properties of concrete, only preliminary results of applying ERT to concrete imaging have been published so far. The aim of this paper is to carry out a feasibility evaluation with specifically cast samples. The results indicate that ERT may be a feasible modality for non-destructive evaluation of concrete.

1. Introduction

Much of America's concrete infrastructure was built with technology dating to the mid-1900s. With the deterioration and failure rates escalating as this infrastructure continues to age, it is critical that better non-destructive techniques are developed to allow early detection of the deterioration process so that proper repair strategies can be applied. Techniques that provide information on the location of the reinforcing bars, the degree of cracking in the reinforced concrete, the distribution of chlorides in the matrix, the humidity gradients in concrete, the state of corrosion, and the depth of cover, are needed. Electrical methods, which vary in terms of costs and ease of use, are well suited for inspection and evaluation of large concrete structures. A number of studies during the last two decades have indicated that electrical measurements carry information on several properties of concrete. Impedance spectroscopy based on using alternate currents (AC) has been applied for detection of cracks [1,2], fiber distributions [3,4], fiber orientations [5], and corrosion rate of reinforcing bars [6–9]. In addition, AC impedance measurements are known to be sensitive to concrete humidity [10,11] and chloride distributions [12,13]. Unfortunately, AC impedance spectroscopy, as well as many other non-destructive evaluation methods, is sensitive to uncertainties and inaccuracies of the models. Especially, the geometry of the target often cannot be modeled accurately. Moreover, the models used in impedance spectroscopy do not take into account spatial variations of concrete conductivity. A comprehensive framework for filtering the information gained from the non-destructive test while accounting for these uncertainties is needed [14].

In Electrical Resistance Tomography (ERT), the geometry and the spatial variations of the conductivity are taken into account [15]. In ERT, a set of electrodes is attached to the surface of the target. Electric current is applied through electrodes, and the potential differences produced on the surface are measured using several electrode pairs. Based on these measurements, the ERT problem is to compute an estimate for the 3D distribution of resistivity (or its reciprocal, conductivity). So far, only a few attempts to applying ERT to non-destructive testing of concrete or other cement-based materials have been reported. In 1994 Daily et al. [16] applied ERT to image reinforced concrete. However, the quality of the reconstructions was not sufficient for practical applications. Buettner et al. [17,18] performed water infiltration tests, which demonstrated that ERT can be used for monitoring the temporal evolution of moisture distribution in concrete structures. More recently, Hou and Lynch [19] showed that ERT is applicable for detection of cracks in fiber-reinforced cement composites. In this paper the results were represented as differences between the conductivity distributions corresponding to cracked samples and the same samples before cracking. This approach was taken in order to remove inhomogeneities from the reconstructions. However, when imaging existing concrete structures, the reference conductivity map of the pre-cracked target is not available, and hence the assessment of cracking should be solely based on the measurements acquired after a (possible) damage.

ERT belongs to the class of diffuse tomography modalities, and the associated reconstruction problem is an ill-posed inverse problem [20,21]. The practical definition of inverse ill-posed problems is that they are drastically sensitive even to moderately small measurement and modeling errors. The overall model for the ERT, the so-called *complete*

* Corresponding author. Tel.: +358 40 7405624; fax: +358 17 162585.
E-mail address: Aku.Seppanen@uku.fi (A. Seppänen).

0008-8846/$ – see front matter © 2009 Elsevier Ltd. All rights reserved.
doi:10.1016/j.cemconres.2009.08.023

electrode model, is generally considered to be adequate to describe the relationship between the measurements and the conductivity distribution [22,23]. The classical approach to deal with inverse problems is to employ regularization methods, such as, Tikhonov regularization. More recently, the Bayesian (statistical) approach to inverse problems has gained popularity [21,24]. In the Bayesian formalism, the uncertainties and errors in the measurements and models, as well as the properties of the unknown conductivity distribution itself, are modeled explicitly. The explicit statistical models for the primary unknown are referred to as *prior models* or *priors*.

In the case of ERT, the uncertainties are mainly related to the exact geometry of the target object and the related electrical boundary conditions, as well as numerical and computational implementation. Many of these have already been at least partially solved, such as numerical model reduction [21,25], simultaneous estimation of contact impedances [26] and the problem of computational domain truncation [27]. As for models for the conductivity distribution, there are several possibilities, such as the classical white noise model, (improper) smoothness priors [28], proper smoothness priors [21], inhomogeneous and anisotropic (structural) smoothness priors [29], total variation priors [30,31], L_1 (impulse) priors [31], and Besov priors [32]. The selection of the prior model depends heavily on the prior information and the assumptions on the target. For example, targets that are results of diffusion processes, are usually modeled as (homogeneous) smoothness processes, while targets, which have small objects embedded in relatively homogeneous background, might be modeled with an L_1 prior model.

In this paper we use ERT for imaging concrete specimens. State-of-the-art computational models and inversion methods are employed in the reconstruction. The study demonstrates that accurate modeling of the measurements and utilizing structural priors can yield accurate reconstructions of the concrete conductivity. While in papers [17–19] reference data corresponding to samples before wetting/cracking was utilized in the reconstructions, we consider cases where reference data is not available. In the experiments of this paper the geometry is quite simple: all the specimens are short cylinders and the electrodes are attached equidistantly around the cylinder surface. However, since ERT is a diffuse tomography modality, it is not always necessary to have access to all boundaries of the target. By contrast, it may be adequate to inject current and measure voltages using an array of electrodes attached to one surface only, see [33]. In Electrical Impedance Tomography (EIT), which is an extension of ERT, the capacitive nature of the target is also modeled and the phase-shifts between the injected currents and measured voltages are also taken into account; see for example [34]. In this paper we ignore the capacitive effects.

2. Electrical Resistance Tomography (ERT)

Electrical Resistance Tomography (ERT) is an imaging modality used to estimate the internal conductivity distribution inside objects on the basis of current injections and voltage measurements acquired from the object boundary. ERT is a diffusive modality, because if a current is injected into the target volume between any two points, the electric current (density) spreads into the whole volume. As a consequence, the image reconstruction is more complicated than, for example, in X-ray tomography, in which the X-rays travel in straight line and one measurement carries information from a very restricted subset of the target. The model for electrical boundary measurements, the forward model of ERT, is reviewed briefly in Section 2.1, and the inverse problem in Section 2.2.

2.1. ERT measurements and the forward model

In ERT, alternating currents I_ℓ are injected through electrodes attached on the surface of the object, and the resulting voltages V_k are measured between different pairs of electrodes (Fig. 1).

The most accurate model for ERT is referred to as complete electrode model [22,23]. Denote the target volume under investigation by Ω, its exterior boundary by $\partial\Omega$ and the patch under the ℓth electrode by e_ℓ. The complete electrode model consists of the Poisson equation

$$\nabla\cdot(\sigma\nabla u) = 0,\ \bar{r}\in\Omega \tag{1}$$

and the following boundary conditions:

$$\int_{e_\ell} \sigma\frac{\partial u}{\partial \bar{n}}dS = I_\ell,\ \bar{r}\in e_\ell,\ \ell = 1,\ldots,L \tag{2}$$

$$\sigma\frac{\partial u}{\partial \bar{n}} = 0,\quad r\in\partial\Omega\setminus\cup_{\ell=1}^{L} e_\ell \tag{3}$$

$$u + \xi_\ell\sigma\frac{\partial u}{\partial \bar{n}} = U_\ell,\ \bar{r}\in e_\ell,\ \ell = 1,\ldots,L \tag{4}$$

where $\sigma=\sigma(\bar{r})$ is the conductivity, $\bar{r}\in\Re^3$, $\bar{r}=(x,y,z)$ is the spatial coordinate, $u=u(\bar{r})$ is the electric potential in the body, U_ℓ is the potential on the ℓth electrode, ξ_ℓ is the contact impedance between the ℓth electrode and the object, and $\bar{n}$ is an outward unit normal. The boundary conditions (2)–(4) can be interpreted in the following way: $\sigma\frac{\partial u}{\partial \bar{n}}$ is the current density through the boundary and hence Eq. (2) indicates that the integral of the current density over the ℓth electrode is equal to total current I_ℓ through the electrode. Furthermore, the boundary condition defined in Eq. (3) implies that there are no currents through the electrode-free boundary. Eq. (4) represents the boundary condition for the electric potential. If the electric contact between an electrode and the target surface was perfect, the electric potential u under each electrode e_ℓ would be constant and equal to U_ℓ. The contact impedance ξ_ℓ, however, causes a potential drop equal to $\xi_\ell\sigma\frac{\partial u}{\partial \bar{n}}$ between the electrode and the target surface.

In addition, the currents I_ℓ need to satisfy the charge conservation condition

$$\sum_{\ell=1}^{L} I_\ell = 0 \tag{5}$$

and the potential reference level has to be fixed, for example by writing

$$\sum_{\ell=1}^{L} U_\ell = 0. \tag{6}$$

By approximating the complete electrode model (1)–(6) numerically for example using the finite element method (FEM), the model can be written in the form

$$V = R(\sigma,\xi)I + v = R^*(\sigma,\xi) + v, \tag{7}$$

where V, I, ξ and v are vectors consisting of voltage measurements (potential differences between selected electrodes), currents, contact impedances, and observation noise, respectively. Here, σ denotes a finite dimensional approximation for the conductivity distribution. The function $R^*(\sigma,\xi)$ which maps the electrode currents to voltages, is linear with respect to electric current I but non-linear with respect to σ and ξ. For the implementation of the FEM model used in this paper, see [35].

2.2. Inverse problem in ERT

The previous section discussed the forward model of ERT. The forward problem of ERT – computing the boundary voltages given the conductivity distribution, contact impedances and electrode currents –

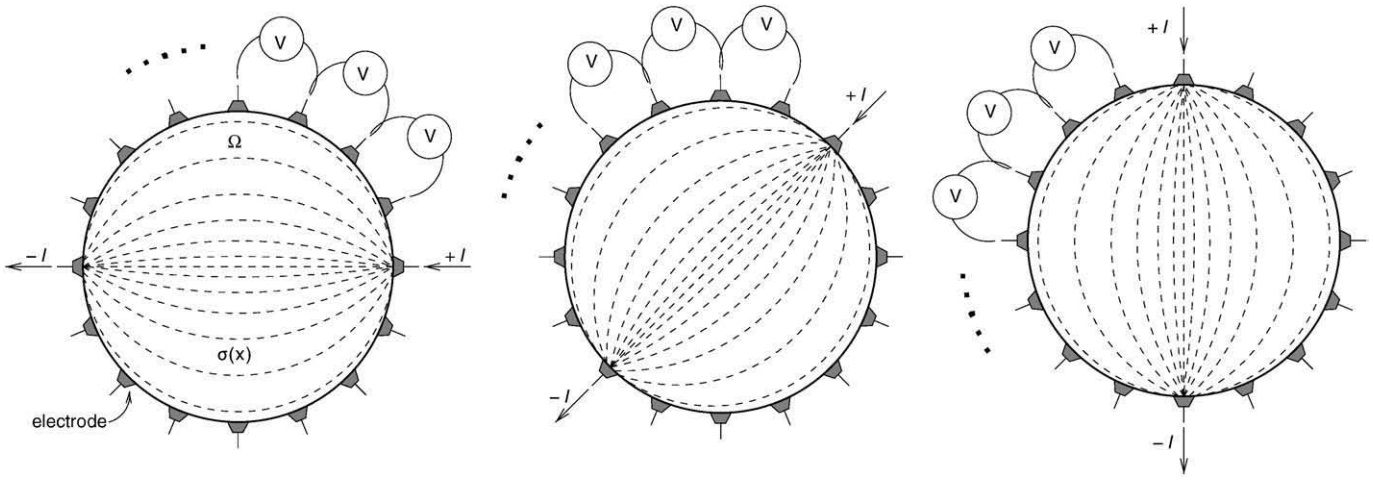

Fig. 1. An example of voltage measurements corresponding to three current injections in ERT.

is a mathematically well-posed (stable) problem. The inverse problem of ERT, that is, reconstructing the internal conductivity distribution and the contact impedances given the boundary voltage measurements, is an ill-posed inverse problem. This implies that the solution of the inverse problem is not unique, and it is sensitive to modeling errors and measurement noise. Hence, the solution of the inverse problem requires special methods.

The reconstruction methods in ERT can be divided in deterministic and statistical methods. In the deterministic approach, the ill-posed inverse problem is replaced by a well-defined problem that is stable and has a unique solution. This procedure is referred to as *regularization* [20]. In a statistical approach, an explicit prior model for the target is written, and the solution of the inverse problem is sought via the *a posteriori* distribution, which combines the prior and measurement models and the information given by the measurements [21,24].

If the measurement noise v can be assumed to be Gaussian with zero mean and covariance C_v, and to be independent of the conductivity, the *likelihood (measurement) model* is of the form $\exp\left(-\frac{1}{2}\left\|L_v(V-R^*(\sigma,\xi))\right\|^2\right)$, where $L_v^T L_v = C_v^{-1}$. Furthermore, if the prior model is exponential with a distribution $\exp(A(\sigma,\xi))$, the posterior distribution of the conductivity and the contact impedances given the measurements is of the form $p(\sigma,\xi|V)\propto \exp(\Xi(\sigma,\xi;V))$, where

$$\Xi(\sigma,\xi;V) = \left\|L_v(V-R^*(\sigma,\xi))\right\|^2 + A(\sigma,\xi). \tag{8}$$

A typical choice for the *prior potential* $A(\sigma,\xi)$ has the form

$$A(\sigma,\xi) = \alpha_1 \int_\Omega |\kappa\nabla\sigma|^2 d\Omega + \alpha_2\left\|\xi-\xi^*\right\|^2 \tag{9}$$

where $\kappa\in\Re^{3\times 3}, \kappa=\kappa(\bar{r})$ is a positive semidefinite matrix (field), which operates on the gradient of conductivity. In the regularization theory and related methods, the prior potential corresponds to regularization functional. In regularization theory, however, the procedure and the overall philosophy of selecting the regularization functional are completely different from the construction of the prior model. If κ is an identity matrix, the first term of the prior potential is simply $\alpha_1\int_\Omega |\nabla\sigma|^2 d\Omega$, and this prior potential increases with increasing spatial variations in σ. As a consequence, this choice for $A(\sigma,\xi)$ results in spatially smooth reconstructions. For this reason, the associated prior is referred to as *smoothness prior*. In the case of imaging concrete, however, the conductivity distributions are necessarily not smooth: reinforcement bars and cracks correspond to stepwise changes in the conductivity distribution. Such structures can be modeled with (*inhomogeneous*) *anisotropic smoothness priors*, which imply uneven smoothness assumptions in different directions. Anisotropic smoothness in different directions is achieved by a specific construction of the matrix κ. Anisotropic smoothness prior is a versatile concept that can be applied to many cases, especially in such cases in which we have prior information on the orientation of internal structures. The idea of anisotropic smoothness prior is illustrated in Fig. 2. For details, see [21,29].

In Eq. (9), ξ^* is a vector including expected values for contact impedances. Therefore, the second term in the penalty functional favors the contact impedances close to expected values. The scaling parameters $\alpha_1,\alpha_2\in\Re$ represent the uncertainty of variations of the conductivity smoothness and the contact impedances, respectively. For example, very high value for α_1 corresponds to assuming that the conductivity distribution is an almost constant in the target domain. The selection of the scaling parameters is usually based on separate experiments and Monte Carlo simulations.

The most common *point estimate* for the unknowns is the *maximum a posteriori (MAP) estimate*. This is usually computed as the minimizer of the posterior potential $\Xi(\sigma,\xi;V)$. The minimizer of $\Xi(\sigma,\xi;V)$ is often computed by using the Gauss–Newton algorithm equipped with a line search algorithm and a projection algorithm for the positivity constraints [36,37]. For different optimization methods applied to ERT, see for example [38].

The (anisotropic) smoothness prior is not always a feasible prior model when the target conductivities span several orders of magnitude or contain stepwise changes. A reinforced concrete structure is such a target. In these cases, the *logarithmic parametrization* for the conductivity can be used. That is, we write the prior and likelihood models in terms of $\beta=\ln(\sigma)$ and compute the MAP estimate for β. Then, the conductivity $\sigma=\exp(\beta)$ is calculated based on the MAP estimate. This prior yields conductivity distributions that are smooth in the logarithmic scale and thus allow for variations of several orders of magnitude. Furthermore this parametrization yields an implicit positivity constraint for σ. For the logarithmic parametrization scheme in the context of thermal diffusion tomography, see [39].

Above the ERT inverse problem was considered in the case of unknown contact impedances ξ. Conventionally in ERT, the contact impedances are assumed to be known, and the aim is to reconstruct only the (discretized) conductivity distribution σ on the basis of voltage measurements V. However, the inaccuracies of the contact impedances can cause significant errors in the conductivity reconstructions. This is the case especially when imaging concrete, because the contact impedances between the electrodes and concrete surface can vary considerably. An alternative approach in which the contact

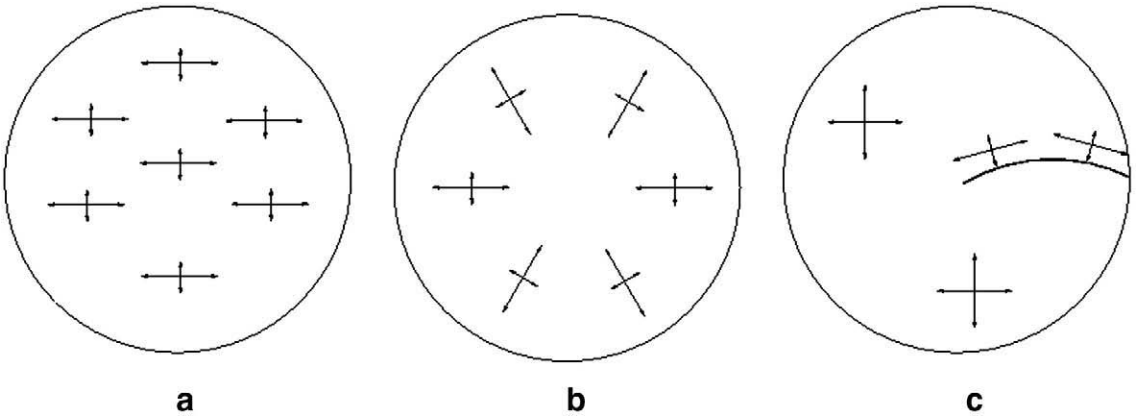

Fig. 2. Three different anisotropic smoothness priors. The cross arrows illustrate the eigenvectors of κ multiplied by the corresponding eigenvalues. High eigenvalue implies high smoothness in the direction of the corresponding eigenvector. a) High smoothness in the direction of x-axis. b) High radial smoothness. c) Anisotropic smoothness along a fault line and isotropic smoothness elsewhere.

impedances ξ are estimated simultaneously with the conductivity distribution was introduced in [26].

3. Experiments

In order to validate the feasibility of ERT to imaging of concrete, several specimens with controlled inhomogeneities were cast and the specimens were measured nine days after casting. The measurements were carried out with EIT-instrument developed in University of Kuopio. The reconstructions were computed following the scheme described in Section 2. The reconstruction software (including also the FE package for forward computations) is an adaptation of the implementations described in [26,29,35,40,41]. In reality, a moisture gradient also induces a significant conductivity gradient. In this feasibility assessment, however, we limit ourselves to investigating how well structural inhomogeneities such as rebars and cracks can be detected from a more or less uniformly conducting background.

3.1. Specimens

Short cylindrical specimens were cast (15 cm in diameter, 3 cm high). Concrete had the following mixture proportion: aggregates (83%), Portland cement (15%), and fly ash (2%) by mass. The maximum size of the aggregate was 8 mm and a w/c ratio of 0.8 was used, resulting in a compressive strength of 20–25 MPa. Different types of objects were cast inside the specimens: Case 1: polyurethane block, Case 2: vertical steel bar, Case 3: horizontal steel bar, and Case 4: plastic plates. These objects were chosen to provide contrast with respect to the concrete conductivity. After casting, the molds with the concrete samples were sealed airtight until the concrete specimens were hardened enough to be removed from their molds. Next, the specimens were covered with plastic in order to maintain uniform humidity in each concrete cylinder. The measurements were carried out nine days after casting. While the resistivity of mature concrete in indoor climate can exceed 10,000 Ωm [42], the cast specimens were young and saturated and the measured bulk resistances were always below 10 kΩ.

3.2. Measurement equipment

The ERT measurements were carried out using a Kuopio impedance tomography (KIT4) device, which is an Electrical Impedance Tomography measurement system built for industrial process tomography applications [43].

To get electrical contact to concrete, we used wet copper–copper sulphate (Cu–$CuSO_4$) electrodes, similar to those described by Monteiro et al. [6]. One of the electrodes is shown in Fig. 3a. With Cu–$CuSO_4$ electrodes, the electrical contact is obtained by attaching a wet sponge to the concrete surface. The sponge is wetted with copper sulphate solution, which is stored inside a hollow copper cylinder covered by a plastic casing. The current and voltage cords to KIT4 instrument were connected to the copper cylinders. The electrodes were pushed towards the concrete surface with springs. The advantages of using Cu–$CuSO_4$ electrodes are: (1) the wet sponge ensures a sufficient electrical contact to concrete, and (2) the polarization between copper and copper sulphate is low.

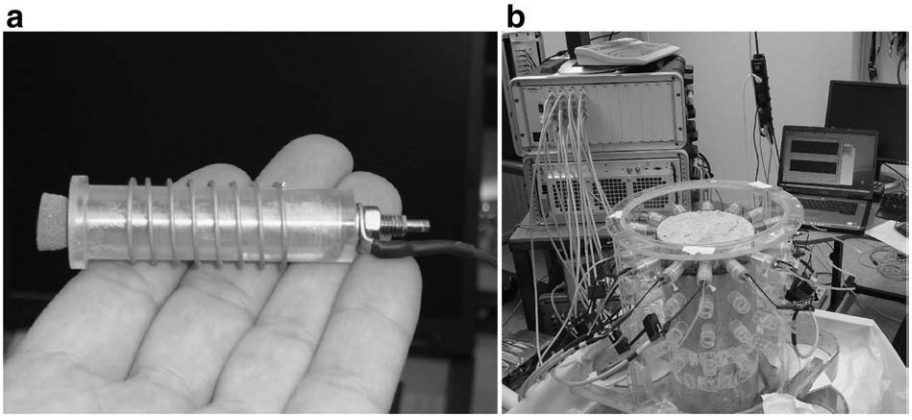

Fig. 3. a) A wet electrode. b) KIT4 measurement system, and the experiment setup. The specimen lies on top of a pile from which it is electrically insulated.

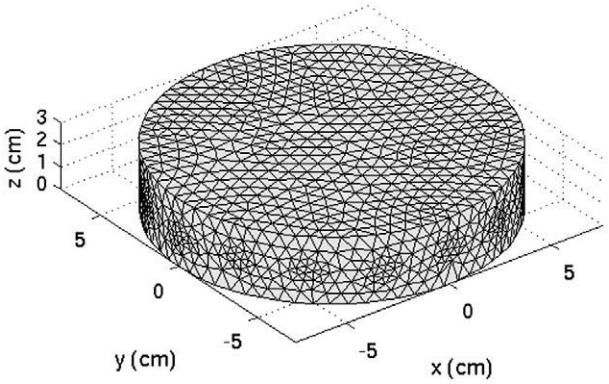

Fig. 4. FEM grid used in modeling the measurements.

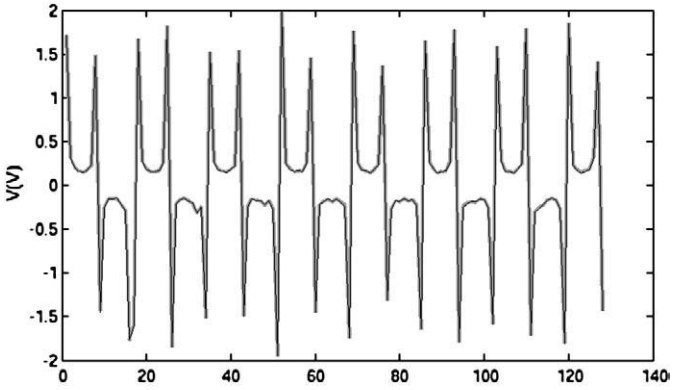

Fig. 6. Case 1. Measured EIT data (thick gray line) and the computed data (black line).

The ERT measurements were acquired through the use of 16 electrodes that were placed equidistantly around the concrete samples, see Fig. 3b. The electrical currents were sinusoidal (amplitude 1 mA, frequency 1 kHz), and the currents were injected between 8 opposite electrode pairs, as illustrated in Fig. 1. Corresponding to each current injection, the voltages were measured between all adjacent electrode pairs (including also the current-carrying electrodes); the number of voltage measurements per specimen was thus 8.16 = 128.

3.3. Computational aspects

For the specimens with embedded metals, logarithmic parametrization was used; for all the other cases, isotropic/anisotropic smoothness priors were used. Fig. 4 shows a surface plot of the mesh used in finite element approximation of the ERT forward model. The mesh contains 11,574 elements. In the FEM scheme, the conductivity was represented in a piecewise linear basis, and the electrical potential u inside the target was approximated with a piecewise second order polynomial basis. For the computation of the MAP estimate, the Gauss–Newton algorithm with a line search algorithm was used.

4. Results and discussion

4.1. Case 1: Resistive block

The first specimen which contained a polyurethane block, is shown in Fig. 5a. The block was positioned off-center in the horizontal plane, and placed vertically through the concrete cylinder. Polyurethane, being an electrically insulating material, should produce contrast with respect to conductivity. The reconstruction (Fig. 5b) was computed using an isotropic smoothness prior model. Because the targets lay flat, and the variations in conductivity in the vertical direction were relatively small; only a surface plot of the reconstructed conductivity is drawn.

In the reconstructed conductivity distribution, the resistive volume (conductivity ~0–0.05 mS cm^{-1}) is roughly at the location of the polyurethane block. The background conductivity, i.e. the conductivity of concrete, varies between 0.2 and 0.44 mS cm^{-1}, which is of the same order as the conductivity of concrete given in literature: According to McCarter et al. [44] the resistivity of (0–120 days old) concrete during water curing varies approximately between 15 and 35 Ωm. The corresponding conductivities are 0.28 and 0.67 mS cm^{-1}. The conductivity of concrete is highly dependent on the concrete porosity and the degree of water saturation of the pore space, and therefore the samples were sealed with plastic in order to prevent evaporation of water. We note, however, that the conductivity of concrete is never homogeneous. The aggregate particles are essentially insulating bodies, and the free water in pore space is the conductive phase [42]. Furthermore, the cement paste in the interfacial transition zone around aggregates has a significantly higher porosity than bulk cement paste [14]. As a consequence, the conductivity of the cement paste is not homogeneous, even in homogeneous humidity conditions. If the dimension of the volume to be reconstructed is large, the local variations of the conductivity do not have a significant effect on the reconstructions. On the other hand, if the dimension of an inhomogeneous inclusion is small, the local variations (large

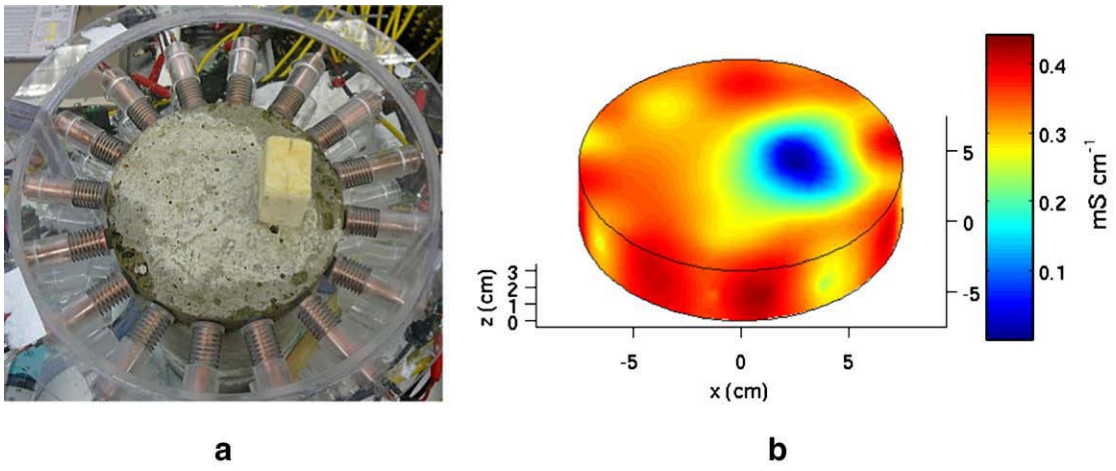

Fig. 5. Case 1. a) A specimen including a resistive polyurethane block. b) The ERT reconstruction.

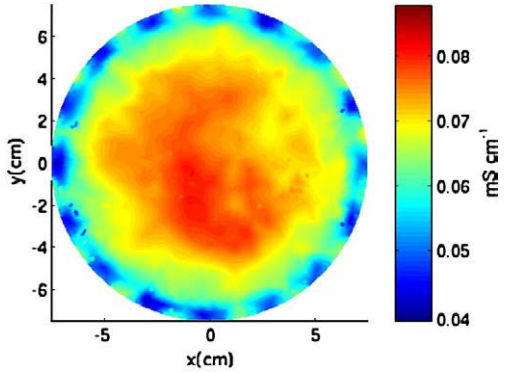

Fig. 7. Case 1. Square root of the posterior variances corresponding to cut-off plane $z = 1.5$ cm.

aggregates, for example) can show up in the reconstructions. How small inclusions can be detected in theory will depend on the employed prior model, the quality and noisiness of the measurements as well as the employed estimation approach, see [31] for an example of superresolution when L_1-prior models and Markov chain Monte Carlo computations are performed. The dimensions of inclusions in these experiments were relatively small, and the inhomogeneities noted in the reconstructions may be the result of large aggregates, air voids, or even non-uniform thickness of the samples. The main reason for the background conductivity variations here, however, is the fact the copper sulphate solution was absorbed by concrete from the wet electrodes. That is the reason for high conductivities in the neighborhood of the concrete boundary. The same phenomenon appears also in the following example cases. This was verified by carrying out consecutive measurement cycles which showed an increase in the conductivities under the electrodes when more and more copper sulphate was absorbed.

Fig. 6 illustrates the measured ERT data and the computed voltages corresponding to estimated conductivity distribution and contact impedances. The computed voltages match very well with the measured voltages, indicating that the forward model of ERT is accurate.

Fig. 7 represents the square root of the posterior variances of the conductivities. Posterior variance defines the level of uncertainty of the estimated conductivities. The variances increase towards the central axis of the cylinder. Further, the uncertainty is lowest under the electrodes. This is due to the fact that the measurements are most sensitive to conductivities in the neighborhood of the electrodes. For computation of the posterior covariance matrix, see [21].

4.2. Case 2: Vertical steel bar

The second specimen contains a vertically oriented steel rod (diameter 3 cm). The position of the steel rod was approximately the same as that of the polyurethane block in the previous case. In the reconstruction, isotropic smoothness prior with logarithmic parametrization was used. The logarithmic parametrization was selected due to the large contrast in conductivity. The result is shown in Fig. 8. The steel bar is localized relatively well. The reconstructed concrete conductivity varies between 0.2 mS cm^{-1} and 0.6 mS cm^{-1}. Here, the contrast is more apparent than in the case of polyurethane block, because of the high conductivity in the metal. Note that the conductivity of the steel is in the range of 10^5 S cm^{-1}, which is significantly higher than the peak value 1.5 mS cm^{-1} in Fig. 8b. The fact that conductivity of steel bar is highly underestimated is a result of two effects. First, the contact impedance between concrete and the steel bar is not taken into account in the model (1–4). The contact impedance causes a potential drop on the interface of the concrete matrix and the steel bar, and when this phenomenon is not taken into account, the conductivity in the location of the steel bar is underestimated. The most important reason, however, is that the boundary voltage measurements are not sensitive to conductivity contrast above some limit. This means that in a background of 0.2 mS cm^{-1} we are not necessarily able to *distinguish* between 2 mS cm^{-1} and 20 mS cm^{-1} inclusions. We are, however, able to *detect* a 20 mS cm^{-1} inclusion in a 2 mS cm^{-1} background.

4.3. Case 3: Horizontal steel bar

In the third experiment, a horizontally oriented steel bar (diameter 1 cm, length 7 cm) was cast inside a concrete sample. The location of the bar is indicated in Fig. 9a by the black marks. The bar is aligned with x-axis, and altitude of the bar central axis is 1.5 cm, that is, vertically the bar is located in the center of the concrete cylinder. As in the previous case, logarithmic parametrization was used. We assumed that the orientation of the bar was approximately known, which enables one to employ an anisotropic smoothness prior. This kind of prior information somewhat improves the quality of the reconstructions. The anisotropic smoothness prior is, however, not very sensitive to inaccuracies in the selected smoothness priors [29].

Again, the contrast between the conductivities of the steel and concrete is high, and the location and size of the bar are quite well tracked. Note, however, that the vertical coordinates of the bar cannot be localized using the data acquired in this experiment, because all the electrodes were placed on a single layer and the measurement geometry thus is symmetrical with respect to the center plane of the

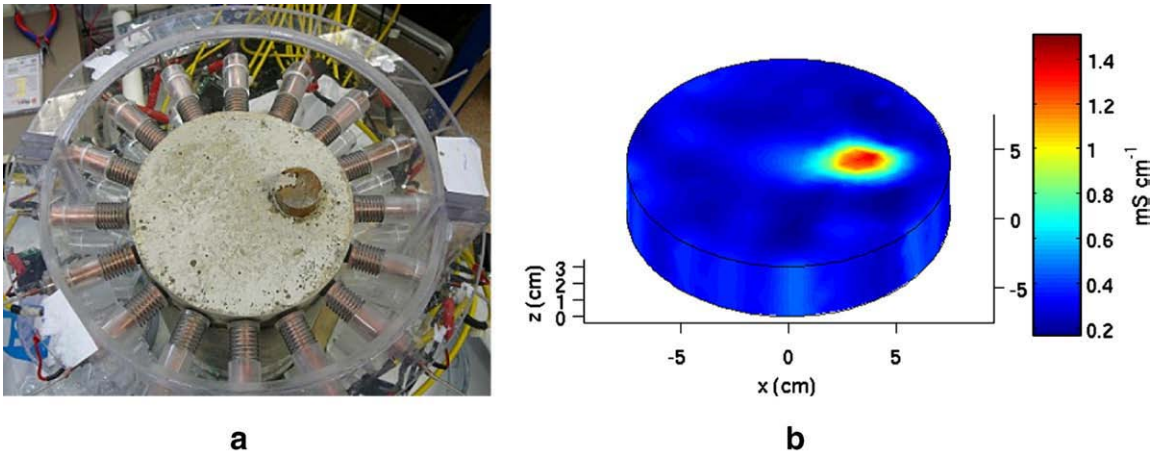

Fig. 8. Case 2. A steel rod cast in concrete. a) The specimen. b) The reconstructed conductivity distribution.

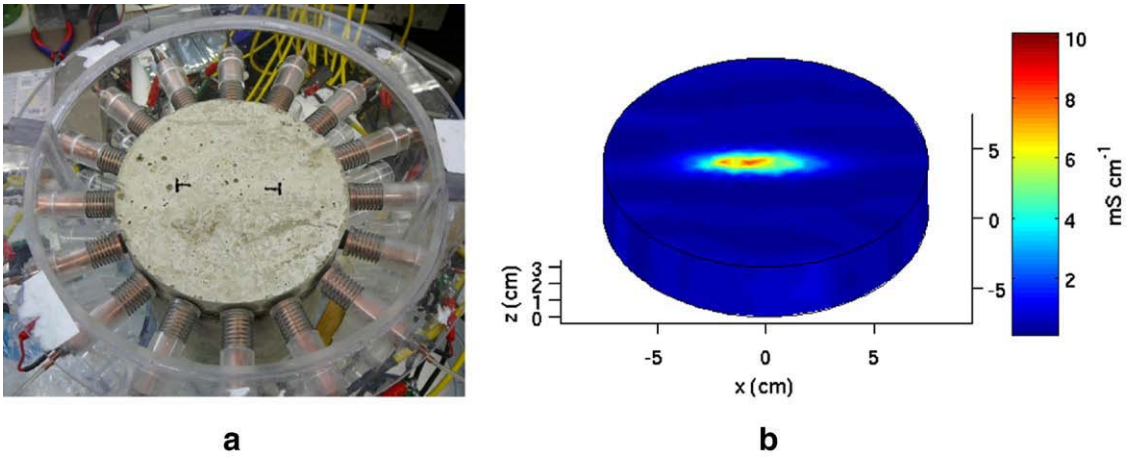

Fig. 9. Case 3. a) A specimen including a horizontal steel bar. Direction of the bar is from left to right. The ends of the bar are indicated in the photo with black marks. b) The reconstructed conductivity distribution.

specimen. For this reason the depth of the bar cannot be estimated (with this measurement geometry).

4.4. Case 4: Plastic plates

In the last experiment, two plastic plates (6 cm and 3 cm wide, both 2 mm thick) were cast inside concrete samples. The specimens and the reconstructions are shown in Fig. 10.

The reconstructed conductivity of both plastic plates was close to zero, which was the desired result because the plates acted as insulators. The difference between the depths of the non-conductive regions in the two reconstructions is clear (Fig. 10b and d). In the reconstruction, anisotropic smoothness prior with assumption of high smoothness in *x*-direction was used. The anisotropic smoothness was written on the boundary in the neighborhood of the plate (30° angle) and in the whole interior of the samples. For the rest of the boundary,

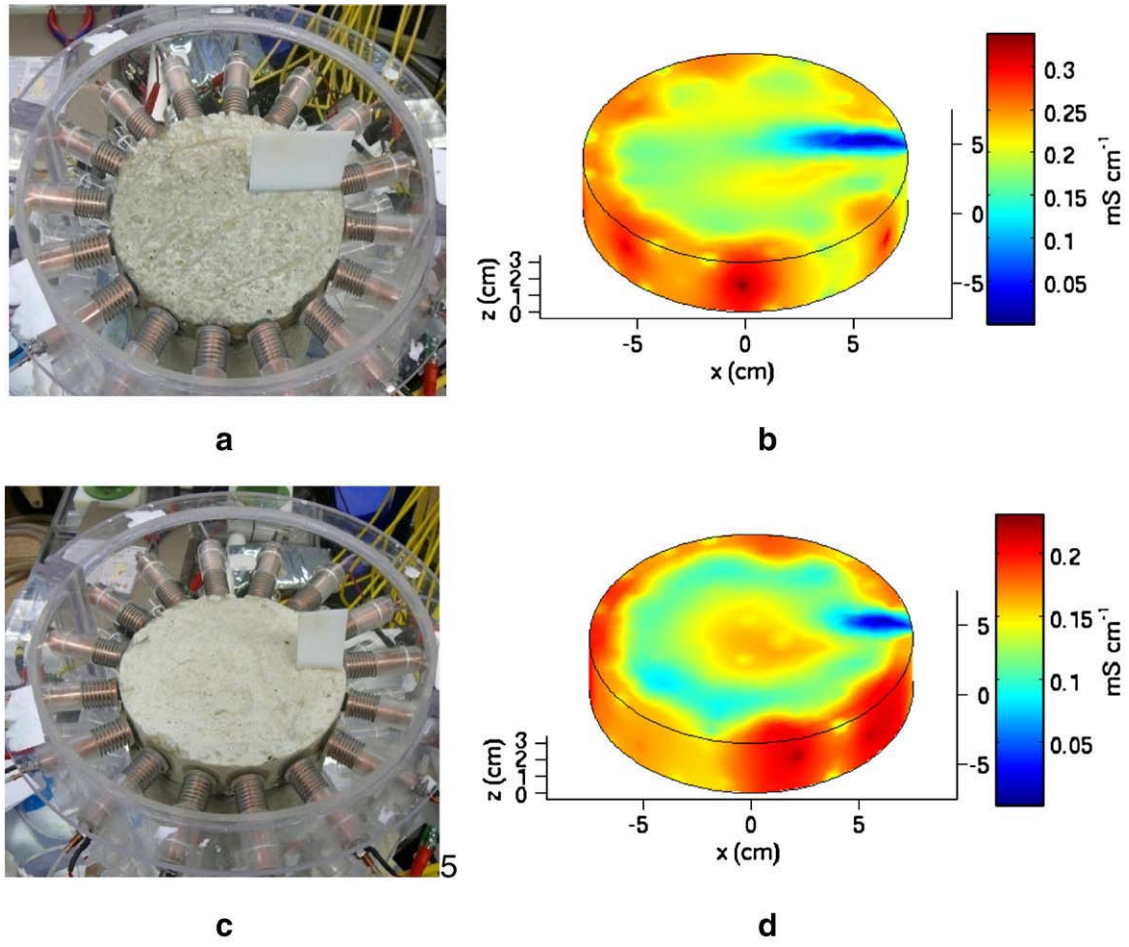

Fig. 10. Case 4. a) and b) specimen with 6 cm wide plastic plate and the reconstructed conductivity distribution. c) and d) specimen with 3 cm wide plastic plate and the corresponding reconstruction.

the conductivities were assumed to be smooth along the concrete surfaces. Again, this type of structural prior information improves the accuracy of the reconstruction. This experiment demonstrates that it is possible to estimate the depth of cracks in concrete using ERT. Note, however, that real cracks can be either resistive or conductive depending on the moisture conditions [1].

5. Conclusions

This paper demonstrates the applicability of using ERT for evaluating the properties of concrete. Concrete specimens cast with a polyuretane block, horizontal steel bar, a vertical steel bar, and plastic plates were measured using ERT. The results indicate that different types of inclusions can be detected and localized using this method. Potential applications of ERT in the construction industry include detection of the thickness of the concrete cover on top of reinforcement bar and estimation of crack depths and moisture distributions. In addition, the information of the reinforcement bars location provided by ERT could be utilized in diagnosing the corrosion rate of reinforcement bars.

The experiments were carried out using young samples that were relatively conductive. However, the ERT imaging scheme is not limited to conductive targets only. By contrast, ERT has been successfully applied to various geophysical problems in which the targets are highly resistive; see for example [45–47].

In this series of experiments, all the samples were short cylinders and measurements were acquired around the target. The next step is to verify the results by measuring concrete slabs from one side only. Our preliminary results have indicated that similarly reliable results can be achieved using measurements from one face of a slab [48]. Another topic of future research is the accounting for the phase-shift data in the reconstruction. This extension leads to reconstruction of complex admittivity distribution in concrete, instead of conductivity distribution.

Acknowledgements

This study was supported by TEKES (Contract No. 40370/06), and the Academy of Finland Centre of Excellence in Inverse Problems Research.

Paulo Monteiro wishes to acknowledge the financial support given by Award No. KUS-l1-004021, made by King Abdullah University of Science and Technology (KAUST).

References

[1] J.F. Lataste, C. Sirieix, D. Breysse, M. Frappa, Electrical resistivity measurement applied to cracking assessment on reinforced concrete structures in civil engineering, NDT & E International 36 (2003) 383–394.
[2] A. Peled, J.M. Torrents, T.O. Mason, S.P. Shah, E.J. Garboczi, Electrical impedance spectra to monitor damage during tensile loading of cement composites, ACI Materials Journal 98 (2001) 313–322.
[3] N. Ozyurt, L.Y. Woo, T.O. Mason, S.P. Shah, Monitoring fiber dispersion in fiber-reinforced cementitious materials: comparison of AC-impedance spectroscopy and image analysis, ACI Materials Journal 103 (2006) 340–347.
[4] L.Y. Woo, N.J. Kidner, S. Wansom, T.O. Mason, Combined time domain reflectometry and AC-impedance spectroscopy of fiber-reinforced fresh-cement composites, Cement and Concrete Research 37 (2007) 89–95.
[5] N. Ozyurt, T.O. Mason, S.P. Shah, Non-destructive monitoring of fiber orientation using AC-IS: an industrial-scale application, Cement and Concrete Research 36 (2006) 1653–1660.
[6] P.J.M. Monteiro, F. Morrison, W. Frangos, Nondestructive measurement of corrosion state of reinforcing steel in concrete, ACI Materials Journal 95 (1998) 704–709.
[7] J. Zhang, P.J.M. Monteiro, H.F. Morrison, Noninvasive surface measurement of corrosion impedance of reinforcing bar in concrete — part 1: experimental results, ACI Materials Journal 98 (2001) 116–125.
[8] J. Zhang, P.J.M. Monteiro, H.F. Morrison, Noninvasive surface measurement of corrosion impedance of reinforcing bar in concrete — part 2: forward modeling, ACI Materials Journal 99 (2002) 242–249.
[9] J. Zhang, P.J.M. Monteiro, H.F. Morrison, M. Mancio, Surface measurement of corrosion of reinforcing bar in concrete — 3: effect of geometry and material properties, ACI Materials Journal 101 (2004) 273–280.
[10] W.J. McCarter, S. Garvin, Dependence of electrical impedance of cement-based materials on their moisture condition, Journal of Physics D: Applied Physics 22 (1989) 1773–1776.
[11] F. Hunkeler, Monitoring of repaired reinforced concrete structures by means of resistivity measurements, Materials Science Forum (Switzerland) 247 (1997) 93–106.
[12] W.J. McCarter, H. Ezirim, AC impedance profiling within cover zone concrete: influence of water and ionic ingress, Advances in cement research 10 (1998) (1998) 57–66.
[13] J.M. Loche, A. Ammar, P. Dumargue, Influence of the migration of chloride ions on the electrochemical impedance spectroscopy of mortar paste, Cement and Concrete Research 35 (2005) 1797–1803.
[14] P.K. Mehta, P.J.M. Monteiro, Concrete: Microstructure, Properties, and Materials, Third edition, McGraw-Hill, 2006.
[15] G.J. Saulnier, R.S. Blue, J.C. Newell, D. Isaacson, P.M. Edic, Electrical Impedance Tomography, IEEE Signal Processing Magazine 18 (6) (2001) 31–43.
[16] W. Daily, A. Ramirez, A. Binley, S. Henry-Poulter, Electrical Resistance Tomography of Concrete Structures, Proceedings of ECAPT94: 3rd European concerted action meeting on process tomography, Lisbon (Portugal), Mar 24–27 1994.
[17] M. Buettner, A. Ramirez, W. Daily, Electrical resistance tomography for imaging concrete structures, Structural Materials Technology an NDT Conference, San Diego, CA (United States), Feb 20–23 1996.
[18] M. Buettner, A. Ramirez, W. Daily, Electrical resistance tomography for imaging the spatial distribution of moisture in pavement sections, Structural Materials Technology an NDT Conference, San Diego, CA (United States), Feb 20–23 1996.
[19] T.-C. Hou, J.P. Lynch, Electrical Impedance Tomographic methods for sensing strain fields and crack damage in cementitious structures, Journal of Intelligent Material Systems and Structures 00 (2008), doi:10.1177/1045389X08096052.
[20] A.N. Tikhonov, A.V. Goncharsky, V.V. Stepanov, A.G. Yagola, Numerical Methods for the Solution of Ill Posed Problems, Kluwer, Dordrecht, 1995.
[21] J.P. Kaipio, E. Somersalo, Statistical and Computational Inverse Problems, Springer-Verlag, New York, 2005.
[22] K.-S. Cheng, D. Isaacson, J.C. Newell, Electrode models for electric current computed tomography, IEEE Transactions on Biomedical Engineering 36 (1989) 918–924.
[23] E. Somersalo, M. Cheney, D. Isaacson, Existence and uniqueness for electrode models for electric current computed tomography, SIAM Journal on Applied Mathematics 52 (1992) 1023–1040.
[24] A. Tarantola, Inverse Problem Theory: Methods for Data Fitting and Model Parameter Estimation, Elsevier, 1987.
[25] J.P. Kaipio, E. Somersalo, Statistical inverse problems: discretization, model reduction and inverse crimes, Journal of Computational and Applied Mathematics 198 (2007) 493–504.
[26] T. Vilhunen, J.P. Kaipio, P.J. Vauhkonen, T. Savolainen, M. Vauhkonen, Simultaneous reconstruction of electrode contact impedances and internal electrical properties, part I: theory, Measurement Science & Technology 13 (2002) 1848–1854.
[27] A. Lehikoinen, S. Finsterle, A. Voutilainen, L.M. Heikkinen, M. Vauhkonen, J.P. Kaipio, Approximation errors and truncation of computational domains with application to geophysical tomography, Inverse Problems and Imaging 1 (2007) 371–389.
[28] D.L. Phillips, A technique for the numerical solution of certain integral equations of the 1rst kind, Journal of the Association for Computing Machinery 9 (1962) 84–97.
[29] J.P. Kaipio, V. Kolehmainen, M. Vauhkonen, E. Somersalo, Inverse problems with structural prior information, Inverse Problems 15 (1999) 713–729.
[30] D.C. Dobson, F. Santosa, An image-enhancement technique for Electrical Impedance Tomography, Inverse Problems 10 (1994) 317–334.
[31] J.P. Kaipio, V. Kolehmainen, E. Somersalo, M. Vauhkonen, Statistical inversion and Monte Carlo sampling methods in Electrical Impedance Tomography, Inverse Problems 16 (2000) 1487–1522.
[32] M. Rantala, S. Vänskä, S. Järvenpää, M. Kalke, M. Lassas, J. Moberg, S. Siltanen, Wavelet-based reconstruction for limited-angle X-ray tomography, IEEE Transactions on Medical Imaging 25 (2006) 210–217.
[33] J. Mueller, D. Isaacson, J.C. Newell, A reconstruction algorithm for Electrical Impedance Tomography data collected on rectangular electrode arrays, IEEE Transactions in Biomedical Engineering 46 (1999) 1379–1386.
[34] P.M. Edic, D. Isaacson, G.J. Saulnier, H. Jain, J.C. Newell, An iterative Newton–Raphson method to solve the inverse admittivity problem, IEEE Transactions on Biomedical Engineering 45 (1998) 899–908.
[35] P.J. Vauhkonen, M. Vauhkonen, T. Savolainen, J.P. Kaipio, Three-dimensional Electrical Impedance Tomography based on the complete electrode model, IEEE Transactions in Biomedical Engineering 46 (1999) 1150–1160.
[36] C.L. Lawson, R.J. Hanson, Solving Least Squares Problems, Prentice-Hall, Inc, 1974.
[37] J. Nocedal, S.J. Wright, Numerical Optimization, Springer Series in Operations Research, Springer, New York, 1999.
[38] P.J. Vauhkonen, Image reconstruction in three-dimensional Electrical Impedance Tomography, PhD thesis, University of Kuopio, Kuopio, Finland, 2004.
[39] V. Kolehmainen, J.P. Kaipio, H.R.B. Orlande, Reconstruction of thermal conductivity and heat capacity using a tomographic approach, International Journal of Heat and Mass Transfer 50 (2007) 5150–5160.
[40] M. Vauhkonen, D. Vadász, P.A. Karjalainen, E. Somersalo, J.P. Kaipio, Tikhonov regularization and prior information in Electrical Impedance Tomography, IEEE Transactions on Medical Imaging 17 (1998) 285–293.

[41] M. Vauhkonen, W.R.B. Lionheart, L.M. Heikkinen, P.J. Vauhkonen, J.P. Kaipio, A MATLAB package for the EIDORS project to reconstruct two-dimensional EIT images, Physiological Measurement 22 (2001) 107–111.
[42] R.B. Polder, Test methods for on site measurement of resistivity of concrete — a RILEM TC-154 technical recommendation, Construction and Building Materials 15 (2001) 125–131.
[43] J. Kourunen, T. Savolainen, A. Lehikoinen, M. Vauhkonen, L.M. Heikkinen, Suitability of a PXI platform for an Electrical Impedance Tomography system, Measurement Science & Technology 20 (2009) 015503 (11pp).
[44] W.J. McCarter, M.C. Forde, H.W. Whittington, Resistivity characteristics of concrete, Institution of Civil Engineers Proceedings 71 (1981) 107–117 pt. 2.
[45] J.E. Chambers, P.B. Wilkinson, A.L. Weller, P.I. Meldrum, R.D. Ogilvy, S. Caunt, Mineshaft imaging using surface and crosshole 3D electricalresistivity tomography: a case history from the East Pennine Coalfield, UK, Journal of Applied Geophysics 62 (2007) 324–337.
[46] F. Nguyen, S. Garambois, D. Chardon, D. Hermitte, O. Bellier, D. Jongmans, Subsurface electrical imaging of anisotropic formations affected by a slow active reverse fault, Provence, France, Journal of Applied Geophysics 62 (2007) 338–353.
[47] E. Piegari, V. Cataudella, R. Di Maio, L. Milano, M. Nicodemi, M.G. Soldovier, Electrical resistivity tomography and statistical analysis in landslide modelling: a conceptual approach, Journal of Applied Geophysics (2009), doi:10.1016/j.jappgeo.2008.10.014.
[48] K. Karhunen, A. Seppänen, A. Lehikoinen, P.J.M. Monteiro, J.P. Kaipio, Crack identification in concrete with Electrical Resistance Tomography, Proceedings of 5th. European Congress on Computational Methods in Applied Sciences and Engineering (ECCOMAS 2008), June 30–July 5, 2008, Venice, Italy.